Geophys. J. R. astr. Soc. (1974) **37**, 73–90.

Synthetic Seismogram Computation by Expansion in Generalized Rays*

Ralph A. Wiggins† and Donald V. Helmberger

(Received 1973 October 18)‡

Summary

The exact formulation of generalized ray theory computations of synthetic seismograms for realistic Earth models is relatively complex and expensive. The expense can be reduced considerably by a proper organization of the computational procedures. The expense is reduced far more dramatically by introducing an approximation of the transmission coefficients and a careful selection of the rays to be included. The incorporation of such procedures leads to programmes which are economically feasible to use as an aid in the interpretation of body waves and near source surface and leaky mode waves.

Introduction

Several recent studies (Helmberger & Wiggins 1971; Gilbert & Helmberger 1972; Helmberger 1972; Wiggins & Helmberger 1973) have described interpretations of seismic observations by making comparisons with synthetic seismograms. The theoretical basis for the computation of such synthetic seismograms has been described by Helmberger (1968) and Gilbert & Helmberger (1972) but the computational procedures and approximations necessary for an efficient implementation have never been published. This paper seeks to rectify this situation by reviewing the theoretical formulas, describing the computational procedures and illustrating the effects of various approximations.

Theory

In this section we will briefly review the integral formulae used to calculate the response of a flat layered half space to a point source. Then we will review the transformation from spherical to flat geometry to show how the case of a point source in a radially heterogeneous sphere may be treated.

As an introduction to the method we consider the propagation of a simple spherical wave in a homogeneous material with wave velocity α. The displacement

* Contribution No. 2376, Division of Geological and Planetary Sciences, California Institute of Technology, Pasadena, California 91109.

† Now at Department of Geophysics and Astronomy, University of British Columbia, Vancouver, Canada.

‡ Received in original form 1973 June 8

potential for a point source assuming a delta function time history can be written

$$\Phi(x, z, t) = (\Psi_0/R) \quad \delta(t - R/\alpha) \tag{1}$$

where $R = (x^2+z^2)^{1/2}$ and Ψ_0 is a constant with units of volume. The Laplace transform of (1) is

$$\Phi(x, z, s) = (\Psi_0/R) \exp [-sR/\alpha] \tag{2}$$

where s is the Laplace transform variable. Using the Sommerfeld (1909) integral, we can write

$$\Phi(x, z, s) = \Psi_0 \int_0^\infty J_0 (kx) \frac{\exp [-(k^2+s^2/\alpha^2)^{1/2} z]}{(k^2+s^2/\alpha^2)^{1/2}} k \, dk, \quad z > 0. \tag{3}$$

Changing variables $k = -isp$, we obtain

$$\Phi(x, z, s) = \Psi_0 (2/\pi) \, s \, Im \int_0^{c+i\infty} \{K_0(spx) \exp [-s\eta_\alpha z] p/\eta_\alpha\} \, dp \tag{4}$$

where $\eta_\alpha = (1/\alpha^2 - p^2)^{1/2}$. The branch cuts introduced by η_α are given in Fig. 1. The integral is convergent in the domain $-1/\alpha < c < 1/\alpha$. The evaluation of (4) is simplified considerably by expanding $K_0(spx)$ in an asymptotic series

$$K_0(spx) = (\pi/2spx)^{1/2} \exp [-spx] \{1 - 1/8spx + 0(spx)^{-2}\} \tag{5}$$

and using only the first term. We then obtain

$$\Phi(x, z, s) = \Psi_0 (2s/\pi x)^{1/2} \, Im \int_0^{i\infty} \{\exp [-s(px+\tau)] |p^{\frac{1}{2}}| \eta_\alpha\} \, dp \tag{6}$$

where $\tau = z\eta_\alpha$. We now make a simple change of variable $t = px + \tau$, based on an observation by Lamb (1904) that allows us to apply the method of Cagniard (1939, 1962) and de Hoop (1960) to find the transient solution by inspection. Since

$$\Phi(x, z, s) = \int_0^\infty \exp [-st] \Phi(x, z, t) dt$$

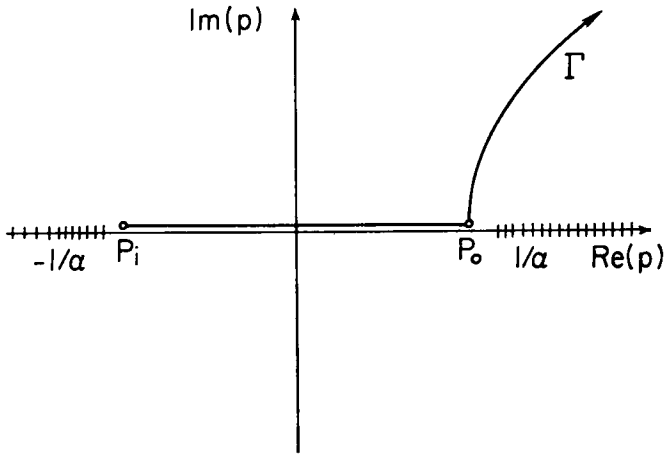

FIG. 1. The Cagniard path and branch cuts for finding the response of a homogeneous fluid to a line source.

we can find $\Phi(x, z, t)$ by deforming the p contour of (6) into the first quadrant in such a way that $t(p) = px+\tau$ is real and increasing. This contour is known as the Cagniard path (see Fig. 1). Along such a path we can write

$$\Phi(x, z, t) = \Psi_0(2/\pi x)^{1/2}\left[\frac{d}{dt}\frac{U(t)}{\sqrt{t}} * H(t)\right] \tag{7}$$

where $U(t)$ is the Heaviside step function, * denotes convolution and

$$H(t) = Im[dp(t)/dt\ p^{1/2}(t)/\eta_\alpha(t)].$$

For the homogeneous problem we can solve for $p(t)$ directly

$$\begin{aligned} p(t) &= t\,x/R^2 - (R^2/\alpha^2 - t^2)^{1/2}\,z/R^2 \quad t \leqslant R/\alpha \\ &= t\,x/R^2 + i(t^2 - R^2/\alpha^2)^{1/2}\,z/R^2 \quad t \geqslant R/\alpha. \end{aligned} \tag{8}$$

The critical points of the contour are located at $p = -z/\alpha R$ ($t = 0$) and $p = x/\alpha R$ ($t = R/\alpha$). We know from (1) that $\Phi(x, z, t) = (1/R)\,\delta(t - R/\alpha)$ so that this provides a simple check on numerical methods used in the evaluation of $\Phi(x, z, t)$.

Now consider the generalization to multiple layers. Fig. 2 illustrates the geometry of the medium. We consider a half space divided into homogeneous layers of thickness h_i with P wave velocity α_i, S wave velocity β_i and density ρ_i. For simplicity we will place the point source Q at the origin and the receiver P at a cylindrical radius x and depth z.

The Laplace transform of the displacement potential for an explosive point source is given by (Strick 1959; Helmberger 1968)

$$\Phi(x, z, s) = \Psi_0(2s/\pi)Im\int_0^{i\infty} K_0(spx)\,\mathscr{B}\,(p, s)\quad (p/\eta_\alpha)\,dp \tag{9}$$

where

p is the seismic ray parameter $\sin i/v$ where i is the angle between the ray and the vertical and v is the velocity;

$\mathscr{B}$ is a function determined by fitting the boundary conditions between the layers and at the surface. These boundary conditions are based on continuity of displacement and normal stress.

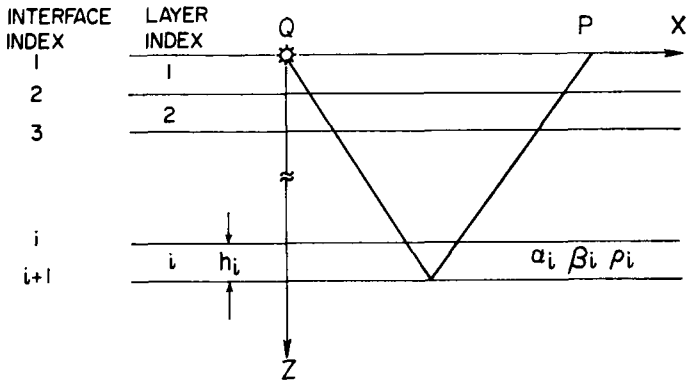

FIG. 2. Definition of layer indexing and co-ordinates for a half space of homogeneous layers.

Helmberger (1967) has demonstrated that $\mathscr{R}$ can be expanded in terms of rays for the case of a layer embedded between two half spaces. Cisternas, Betancourt & Leiva (1973) have demonstrated a general method for expanding $\mathscr{R}$ for a spherical model with many layers. We can write such an expansion symbolically as

$$\mathscr{R}(s, p) = \sum_i \mathscr{R}_i(s, p) \tag{10}$$

$$\mathscr{R}_i(s, p) = \mathscr{F}_i(p) \left\{\prod_j T_j(p)\right\} \left\{\prod_k R_k(p)\right\} \left\{\prod_l \exp\left[-s\, n_l\, h_l\, \eta_l\right]\right\} \tag{11}$$

where

$\mathscr{F}_i$ is the directivity function at the receiver. The vertical u_z and radial u_x displacements can be expressed in terms of the potential solution by taking the time derivative of the potential solution and multiplying by the appropriate directivity function (Gilbert & Knopoff 1961):

$\mathscr{F}$ $= 1$ for the potential solution;

$= 2\eta_\alpha(\eta_\beta^2 - p^2)/\beta^2 D(p)$ for u_z from a P wave or for u_x from an S wave arrival;

$= 4p\eta_\alpha \eta_\beta/\beta^2 D(p)$ for u_x from a P wave or for u_z from an S wave arrival

where $\eta_\alpha = (\alpha_1^{-2} - p^2)^{1/2}$, $\eta_\beta = (\beta_1^{-2} - p^2)^{1/2}$ and $D(p) = (\eta_\beta^2 - p^2)^2 + 4p^2 \eta_\alpha \eta_\beta$ (the Rayleigh function).

T_j are plane wave transmission coefficients across layer boundaries producted over all boundaries crossed by the i'th ray.

R_k are plane wave reflection coefficients at all layer boundaries at which the i'th ray reverses direction.

n_l is the number of times the ray crosses the l'th layer.

h_l is the layer thickness.

η_l $= (v_l^{-2} - p^2)^{1/2}$ where $v_l = \alpha_l$ for p waves or $v_l = \beta_l$ for S waves.

We will normally write this in compact form

$$\mathscr{R}_i(s, p) = R_i(p) \exp\left[-s\tau_i\right] \tag{12}$$

$$\tau_i = \sum_l n_l\, h_l\, \eta_l. \tag{13}$$

The parameter τ is the ' reduced time ' $t - px$ of geometrical ray theory. The reflection and transmission coefficients R_k and T_j are assumed to be selected properly to account for any conversions from P to S or from S to P waves at layer boundaries. Helmberger (1968) gives detailed expressions for the coefficients.

Helmberger (1968) evaluated the integral (9) exactly to find the response of a layered half space. Introduction of the asymptotic expansion (5) for K_0 simplifies the computations considerably. Gilbert & Helmberger (1972) estimate that such an approximation should be adequate in upper mantle studies for p wave pulses shorter than 40 s. Barker (1970) used the first two terms to study near source behaviour of surface waves in a layer over a half space. He studied arrivals at distances up to 10 times the layer thickness (1 km) and examined periods less than 10–20 s. Generally he found that the second term contribution was negligible (private communication).

Substituting (5), (10), (12) and (13) into (9) we have

$$\Phi_i(x, z, s) = \Psi_0 (2s/\pi x)^{1/2}\, Im \int_0^{i\infty} \left\{\exp\left[-s(px + \tau_i)\right] \quad R_i(p) |p^{\frac{1}{2}}| / \eta_\alpha\right\} dp. \tag{14}$$

If we now make the change of variable $t_i = px+\tau_i$ and deform the path of integration to the Cagniard path, we find

$$\Phi_i(x,z,s) = \Psi_0 \left[\frac{2s}{\pi x}\right]^{1/2} Im \int_{t_0}^{\infty} e^{-st} R_i(p)(|p^{\ddagger}|/\eta_a)\frac{dp}{dt}\,dt \tag{15}$$

$$\Phi_i(x,z,t) = \Psi_0 \left[\frac{2}{\pi x}\right]^{1/2} \frac{d}{dt}\,\frac{U(t)}{t^{1/2}} * Im\left\{R_i(p)(|p^{\ddagger}|/\eta_a)\frac{dp}{dt}\right\} \tag{16}$$

$$= G(t) * H_i(t(p))$$

$$\Phi(x,z,t) = \sum_i \{G(t) * H_i(t)\} = G(t) * \sum_i H_i(t)$$

where $U(t)$ is the Heaviside step function and $*$ denotes convolution. If the source had a shape $F(t)$ rather than an impulse we would also need to convolve with $F(t)$.

Let us now consider some geometrical aspects of the problem. According to ray optics, the distance x and travel time t associated with a particular ray with ray parameter p is

$$x(p) = \sum_l n_l h_l p/\eta_l \tag{17}$$

$$t(p) = px + \sum_l n_l h_l \eta_l$$

$$= px+\tau. \tag{18}$$

If we consider only P wave propagation then $\eta_l = (\alpha_l^{-2}-p^2)^{1/2}$. Let p_0 be the value of p for the reflected arrival; i.e. the value of p such that (17) gives the desired x. Also, let $t_0 = t(p_0)$. The Cagniard contour begins at the origin and follows the real axis for $p \leqslant p_0$. At $p = p_0$ the contour leaves the real axis and moves upward into the first quadrant. If the deepest penetration of the ray is to layer L then the branch point of $R(p)$ nearest the origin is $p_1 = 1/\alpha_{\max}$ where $\alpha_{\max} = \max(\alpha_1, \alpha_2 \ldots \alpha_{L+1})$. If $p_1 < p_0$ let $t_H = t(p_1)$ and there is a head wave arrival before the reflected arrival. For $p < p_1$ and real, the integrand of (15) is real and the response is zero. Examples will be given in a following section.

Many of the applications for synthetic-seismogram calculations have been for arrivals from the upper mantle. For such applications the sphericity of the model will significantly effect the results and must be accounted for. Müller (1971) introduced the standard ray-theory Earth flattening transformations for α and β based on physical arguments. Gilbert & Helmberger (1972) demonstrate that these transformations provide an excellent approximation for the calculation of body waves by the Cagniard–de Hoop method. Chapman (1973) has re-examined the problem to try to determine the optimum transformation to use for various modes of propagation. He concludes that a transformation such as proposed by Biswas & Knopoff (1970) is best for SH or SV propagation but was unable to discover an ideal transformation for P wave propagation in a solid.

The ray-theory Earth-flattening transformation that we use is

$$\begin{aligned} v(z) &= p(a) \quad u(r)/r \\ x &= p(a) \quad \Delta\pi/180 \\ z &= p(a) \quad \ln(a/r) \end{aligned} \tag{19}$$

where a is the outer radius of the sphere;

r is the radius of some point within the sphere, $0 < r \leqslant a$;

Δ is the distance measured in degrees;

$p(a) = a/u(a)$.

Since we consider only homogeneous layers in the flat model, the velocity within the layers of the spherical model must be proportional to r. Generally, we apply the same transformation for density as for the velocities. In addition to transforming the radial velocity and density functions, Gilbert & Helmberger (1972) also modify the amplitude by $(\theta/\sin\theta)^{1/2}$ ($\theta = \Delta\pi/180$) to correct for geometrical spreading.

The above summary of the formulae for finding the response of a layered medium is all that is necessary, in principle, to write a computer program. We give here a brief outline of the computational steps. These steps will be elaborated and illustrated in the following sections.

(1) Apply an Earth-flattening transformation to a radially heterogeneous Earth model and then approximate the velocity- and density-depth function with homogeneous layers.

(2) Prescribe the subset of all possible rays for which the calculation should be made.

(3) For each ray perform the following steps: (A) find points along the Cagniard contour in the p plane for which $t(p)$ remains real; (B) find $t(p)$ and $H(t(p))$ for each of the points on the contour; (C) sample $H(t)$ at regular intervals and add to a storage buffer.

(4) Convolve the buffer containing the summed responses of all the rays with $G(t)$ and $F(t)$.

Computational procedures

In this section we describe a number of computational procedures which have proven to be very useful for increasing the efficiency of the computations. These procedures can be grouped into three categories: (1) finding the contour, (2) sampling the amplitude response function, and (3) performing the convolutions.

Finding the contour

For each Cagniard path one must first locate the point p_0, possibly p_1 and points along the Cagniard path. At each of these points one must then find t and dt/dp. Such searches involve the time consuming evaluation of large numbers of complex square roots. The efficiency of the calculations can be improved enormously by expanding t in a Taylor series.

The travel time t for a ray parameter p and distance x is

$$t(p) = px + \sum_l n_l h_l \eta_l$$

where $\eta_l = (v_l^{-2} - p^2)^{1/2}$. Let us consider a change of variables $q^2 = v_m^{-2} - p^2$ ($dq/dp = -p/q$) where v_m is the velocity in the bottom layer penetrated by the ray. Also define $u_l^{-2} = v_l^{-2} - v_m^{-2}$, then

$$\begin{aligned}\eta_l &= (v_l^{-2} - p^2)^{1/2} \\ &= (v_l^{-2} - v_m^{-2} + q^2)^{1/2} \\ &= (u_l^{-2} + q^2)^{1/2}\end{aligned}$$

and we expand with respect to q. The first six derivatives of t with respect to q evaluated at $q = q_0$ are given by

$$a_0 = \sum_l n_l h_l \eta_l$$

$$a_1 = \sum n_l h_l q/\eta_l$$
$$a_2 = \sum n_l h_l v_l^{-2}/\eta_l^3$$
$$a_3 = -3\sum n_l h_l q\, v_l^{-2}/\eta_l^5$$
$$a_4 = -3\sum n_l h_l v_l^{-2}(v_l^{-2}-4q^2)/\eta_l^7$$
$$a_5 = 15\sum n_l h_l q\, v_l^{-2}(3v_l^{-2}-4q^2)/\eta_l^9$$
$$a_6 = 45\sum n_l h_l v_l^{-2}(v_l^{-4}-12v_l^{-2}q^2+8q^4)/\eta_l^{11}.$$

With these coefficients we can evaluate all of the variables needed

$$t = px + \sum n_l h_l \eta_l$$
$$= px + a_0 + a_1\,\Delta q + a_2\,\Delta q^2/2! + a_3\,\Delta q^3/3! + a_4\,\Delta q^4/4! + a_5\,\Delta q^5/5! + a_6\,\Delta q^6/6!$$

$$dt/dp = x - p\sum n_l h_l/\eta_l \quad \text{(fixed } x\text{)}$$
$$= x - p/q(a_1 + a_2\,\Delta q + a_3\,\Delta q^2/2! + \ldots)$$

$$d^2t/dp^2 = -(1/q + p^2/q^3\,(a_1 + a_2\Delta q + a_3\Delta q^2/2! + \ldots)$$
$$+ p^2/q^2(a_2 + a_3\,\Delta q + a_4\,\Delta q^2/2! + \ldots)$$

$$x(p) = p\sum n_l h_l/\eta_l$$
$$= p/q(a_1 + a_2\,\Delta q + a_3\,\Delta q^2/2! + \ldots)$$

$$dx/dq = (-1/p - p/q^2)(a_1 + a_2\,\Delta q + a_3\,\Delta q^2/2! + \ldots)$$
$$+ p/q(a_2 + a_3\,\Delta q + a_4\,\Delta q^2/2! + \ldots)$$

The usual technique is to expand t about some value q_0 and then use the series for values $q = q_0 + \Delta q$ near q_0. Experimental calculations indicate that the error can be estimated quite adequately by the magnitude of $a_6\,\Delta q^6/6!$.

There are two distinct searches. First, given x, the distance to be used for the calculations, we must search for the value p_0 where the Cagniard path leaves the real axis. This search can be made very rapidly using the derivative dx/dq. Once p_0 is located then one must search for the contour by finding points for which $Im(t) = 0$. At each of these points (as well as between p_1 and p_0, if $p_1 < p_0$) the value of $Re(t)$ and dt/dp must be found to be used as components of $H(t)$.

Sampling the response

The procedure outlined above can be used to find values of $H(t)$ at irregularly spaced intervals in time except at p_0. At p_0, the derivative $dt/dp = 0$ and the response becomes infinite. We can find an adequate approximation for the behaviour at the critical point p_0 by expanding t in a Taylor series about t_0

$$t = t_0 + dt/dp(p-p_0) + 0{\cdot}5\,d^2t/dp^2(p-p_0)^2 + \ldots$$

Thus, to first order in $p - p_0$, we have

$$t - t_0 \approx 0{\cdot}5\,d^2t/dp^2 \quad (p-p_0)^2$$

$$dp/dt \approx (t-t_0)^{-1/2} \quad (2d^2t/dp^2)^{-1/2}$$

$$H(t) \approx (t_0-t)^{-1/2}\,Im\{R(p_0)\sqrt{p_0} \quad [2Re\,d^2t/dp^2]_{p=p_0}^{-1/2}\} \qquad t < t_0$$
$$\approx (t-t_0)^{-1/2}\,Im\{R(p_0)\sqrt{p_0} \quad [2Im\,d^2t/dp^2]_{p=p_0}^{-1/2}\} \qquad t > t_0$$

The last two expressions reflect the change of direction of the Cagniard path at p_0. Of course, only the second expression is necessary if there is no head wave arrival. The final '*Re*' and '*Im*' included in the above terms emphasize the fact that the contour bends 90° at $p = p_0$.

In practice, we can never represent the exact shape of the arrival near $t = t_0$. We can, however, find an adequate representation. Since the response function must ultimately be convolved with functions having a finite frequency bandwidth, we need preserve the shape of the response only for low frequencies. Thus, if we compute the shape exactly for times outside a narrow window about t_0 and then replace the $(t-t_0)^{-1/2}$ dependence inside the window by a triangular dependence with the same area, we will have preserved the low frequency characteristics. Such an approximation is illustrated in Fig. 3. The curved line is a layer response $H(t)$ that includes a head wave arrival. The dotted lines indicate how the function goes to $\pm\infty$ at t_0. The solid line has been drawn in such a way that the area between the curve and the axis is preserved.

Once we have determined the response $H(t)$, say by making a spline interpolation of the irregularly spaced time intervals, we are faced with the task of sampling this function at regularly spaced intervals in a way that will avoid aliasing the high frequencies. Such a sampling is necessary if we are to sum the responses of many layers; and since we are dealing with many responses, the sampling must be performed efficiently.

The most obvious sampling method would be first to sample the response at very small increments of time, apply a bandpass filter, and then to decimate. When many layers are being treated this is too time consuming. The sampling process would take longer than generating the functions $H(t)$. Our solution is to bandpass filter by convolving analytically with a triangular function such as one of the ones shown at the bottom of Fig. 3. When the triangular function is just twice the length of the digitization increment, the frequency characteristic is $\sin^2 \omega/\omega^2$ where $\omega = \pi$ is the Nyquist frequency. This filter is very easy to apply and gives a maximum relative

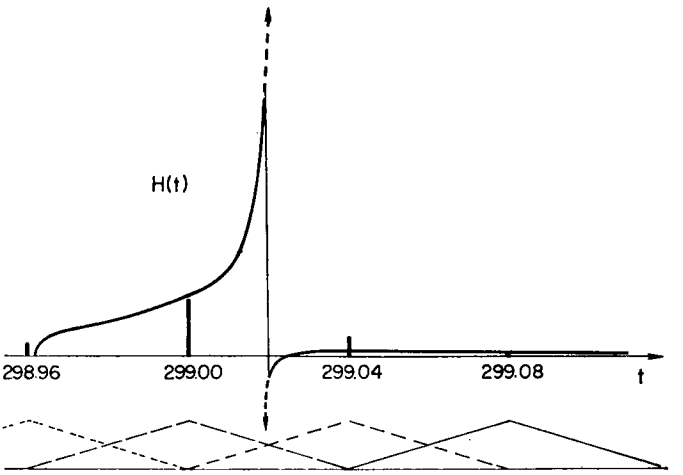

FIG. 3. Sampling functions. Illustration of the technique used for sampling a typical function $H(t)$ to avoid frequency aliasing. The infinite discontinuity in $H(t)$ at $t = t_0$ is replaced by a function that preserves the area in a small finite window around the discontinuity. The continuous function is then smoothed with the triangular functions shown at the bottom before being sampled. The sampled values are illustrated by vertical bars.

aliased power of less than 0·01 for frequencies near $\omega = \pi/2$. In actual practice, the convolution is evaluated only at those times for which a sample value is desired. Thus to obtain the sampled value at time 299·00 s in Fig. 3 we multiply the function $H(t)$ by the triangle located between 298·96 and 299·04 s and integrate to find the sampled value indicated by the bar. This process is repeated at each sample time. Thus we obtain a band-limited representation of $H(t)$.

Convolutions

The responses $H_i(t)$ must be convolved with $G(t)$ and $F(t)$ in order to obtain the final form of the synthetic seismic response. Since both $G(t)$ and $F(t)$ are independent of the geometry of the ray paths and since convolution is associative, the most efficient procedure is to perform the summation $H(t) = \sum H_i(t)$ for all the ray paths and then perform the convolution once for the entire seismogram. This convolution is most conveniently performed by multiplying the Fourier transforms

$$F(\omega)\, G(\omega)\, H(\omega) = \Phi(x, z, \omega)$$

(see for example Stockham 1969). The Fourier transform of $G(\omega)$ is of course just $\Psi_0(2i\omega/\pi x)^{1/2}$.

If, for some reason, one wishes to examine the individual ray responses the most efficient method for convolving $G(t)$ with $H_i(t)$ is to find a rational operator expansion of $G(t)$. Shanks (1967) describes methods for making such approximate expansions. The Z transform of a very good approximation is

$$G(z) = 3{\cdot}7658 - 5{\cdot}3409z + 1{\cdot}6201z^2 - 0{\cdot}13758z^3 + 0{\cdot}11869z^4/(1 - 0{\cdot}81636z)$$

or, in the discrete time domain

$$\phi_i = 3{\cdot}7658h_i - 5{\cdot}3409h_{i-1} + 1{\cdot}6201h_{i-2} - 0{\cdot}13758h_{i-3} + 0{\cdot}11869h_{i-4} + 0{\cdot}81636\phi_{i-1}$$

This type of computation can be carried out more rapidly than the function $H_i(t)$ can be sampled at equally spaced intervals.

Examples

Most of the examples considered in this paper are based on the model shown in Fig. 4. It is very similar to model HWB of Wiggins & Helmberger (1973).

The model was found by a trial and error search of (p, Δ) curves such as shown by the thick smooth line in Fig. 4(b). Each trial curve is first integrated to find the ray theoretical travel times. When a curve is found that is consistent with the travel-time observations it is integrated by the Gerver & Markushevich (1966) modification of the Wiechert–Herglotz integral to find a smooth model of P wave velocity versus radius such as is shown in Fig. 4(a). Suitable S wave and density models are combined with the P wave model and the Earth flattening transformations given in the last section are applied. The models are next converted to a stairstep structure so that the Cagniard–de Hoop technique can be used to calculate the dynamic response to a point source.

The layered structure shown in Fig 4(a) is the unflattened representation of the stairstep model. Layers, that were homogeneous in the Earth flattened representation, now have velocity proportional to r. Except near discontinuities in the smooth model, the layers shown are 20 km thick in the flattened geometry. The (p, Δ) curve corresponding to the stairstep model is shown in Fig. 4(b). Except at discontinuities the stairstep (p, Δ) curve forms a kind of a halo about the original curve.

The dotted lines in Fig. 5 show examples of Cagniard paths for one of the small layers immediately below the low velocity zone. The distances for which these were computed are less than, equal to, and greater than the critical distance $x_1 = 18{\cdot}5°$.

The amplitude functions determined for the layer considered in Fig. 5 are shown in Fig. 6. The seismograms have been aligned for the display. As noted by Müller

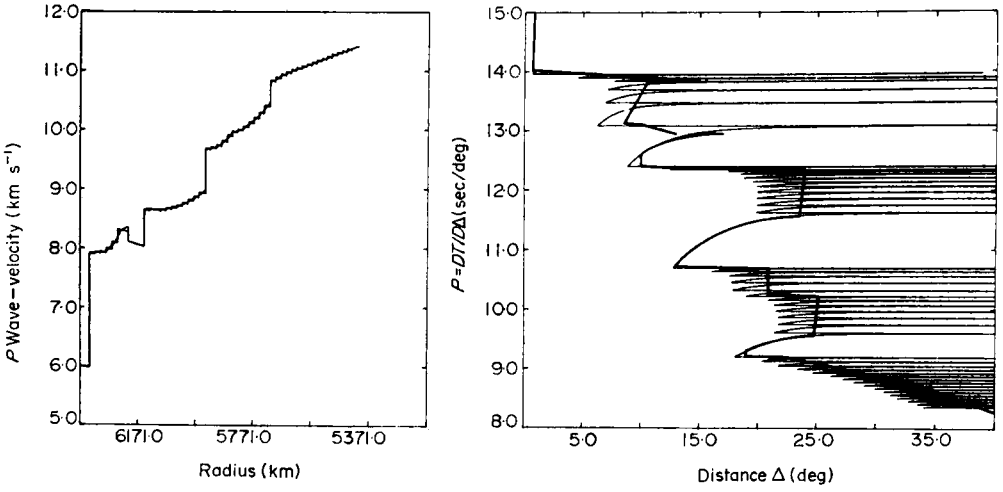

FIG. 4. Velocity-depth and p-delta curves for an upper mantle model that is used for most of the examples. The stairstep velocity structure has steps 20 km thick.

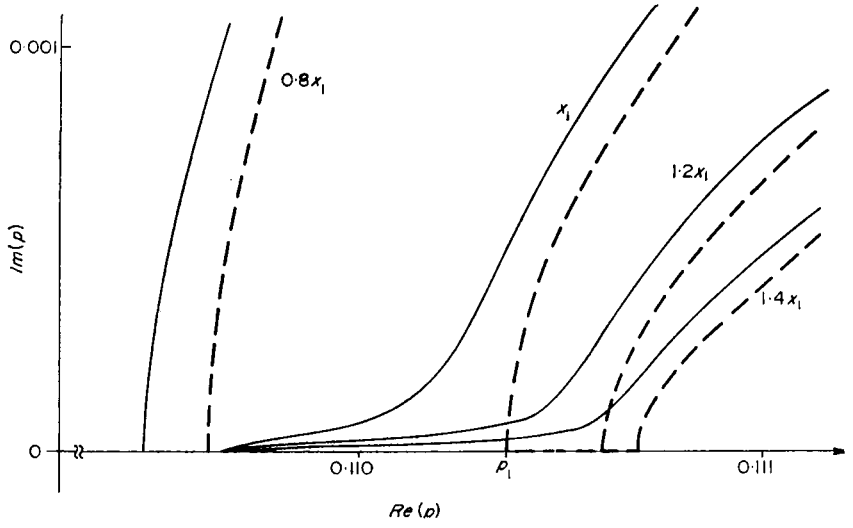

FIG. 5. Cagniard paths for the response of a layer just below the low-velocity zone in Fig. 4. The dotted lines show the paths followed for various radial distances from the source. The solid lines show how the paths are modified by inserting a small high-velocity layer so that the layer in question is in a shadow zone. x_1 is the critical distance for rays corresponding to the dotted lines.

(1970), Fuchs & Müller (1971), Červený & Ravindra (1971) and Müller (1973), among others, the arrivals gradually alter from a delta function for distances much less than the critical angle to a first derivative operator in time for distances much beyond the critical angle. There is no special amplitude feature associated with the critical angle. At some distance beyond the critical angle a separate head wave disassociates from the arrival. The distance depends on the frequency bandwidth of the signal. For very high frequencies (e.g. >500 Hz) the separation can be detected immediately. For frequencies near 1 Hz the separation does not become distinct until beyond $x = 2x_1$.

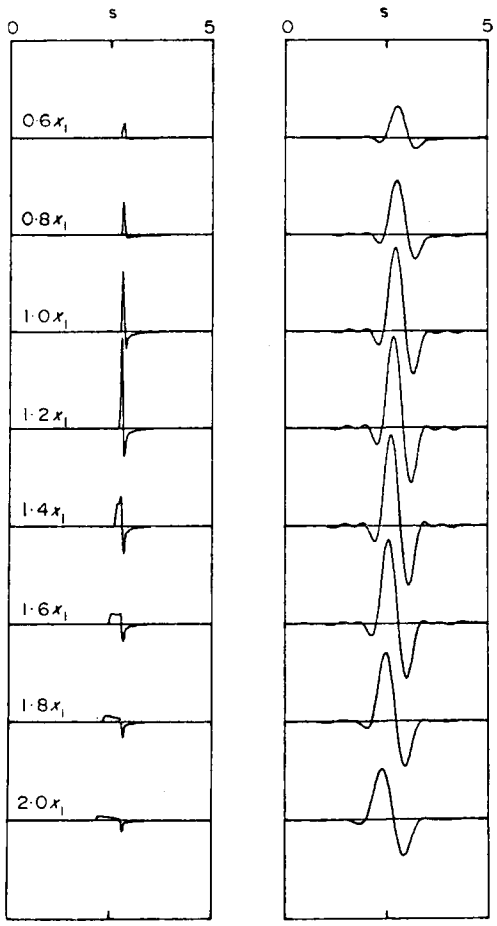

FIG. 6. Potential responses of a layer with a small velocity jump as a function of distance relative to the critical distance x_1. These responses correspond to the dotted Cagniard paths in Fig. 5. Notice that in the filtered (low-pass with cutoff at 1 Hz) representation there is no noticeable change of amplitude or shape associated with the critical distance x_1.

The amplitude functions for a large velocity step are qualitatively similar to those for a small velocity step. The responses in Fig. 7 are from the discontinuity near a depth of 430 km. The principal differences are that the amplitude maximum is much sharper near the critical distance ($x_1 = 12{\cdot}5°$) and the head wave separates from the reflected wave much more quickly.

An interesting example of the generality of the computational procedure is the computation of waves diffracted from a layer within a low-velocity zone (Fig. 8). For this example we modified the velocity-depth function shown in Fig. 4(a) by adding a 2-km layer immediately below the low-velocity zone with a velocity slightly greater than that associated with the arrivals illustrated in Fig. 6. This has the effect of placing the layer in question within a low-velocity zone that does not totally mask its response. The solid lines in Fig. 5 are the Cagniard paths as they are modified by introducing the thin high-velocity layer. The layer and distances used are the same as

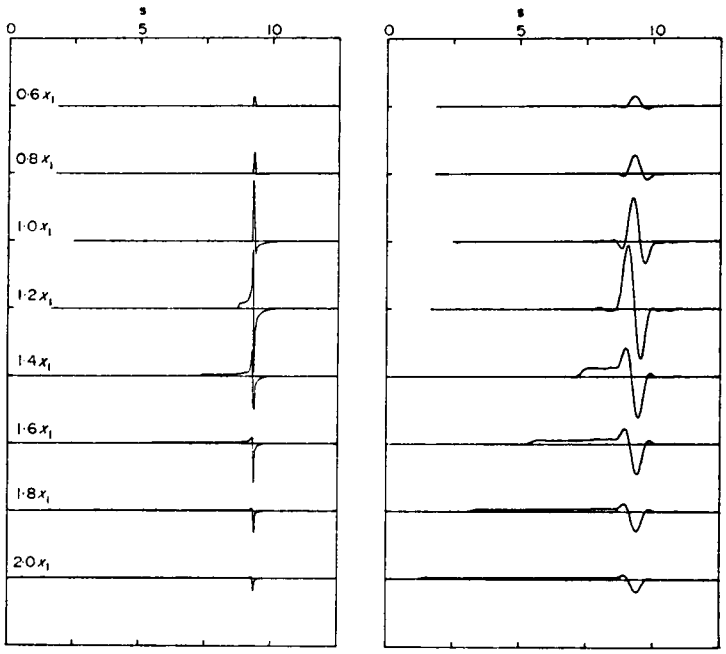

FIG. 7. Potential responses of a layer with a large velocity jump as a function of distance relative to the critical distance x_1.

were used for the dotted lines. The paths all leave the real axis to the left of $1/\alpha_{max}$ where α_{max} is the velocity of the high-velocity layer. They then bend over and are displaced to the right until they can follow a path nearly parallel to the dotted lines. The major energy in the responses shown in Fig. 8 is associated with the region of the contour where it is bending away from the real axis. Notice that the computed responses contain primarily low-frequency energy and that there is little or no phase distortion.

Another example of generalized ray computations is the generation of Rayleigh waves. For this example we consider a point source located 10 km below the surface of a homogeneous half space. This problem is similar to a problem considered by Pekeris *et al.* (1965). Fig. 10 shows the vertical and radial displacements computed using only the direct ray. Some of the corresponding Cagniard paths are illustrated in Fig. 9. The development of the Rayleigh wave is directly related to the nearness of the contour to the Rayleigh pole that is introduced by the directivity function. It is surprising to see the Rayleigh wave beginning to develop even for $x = 25$ km. A similar phenomenon can be seen in the results of Pekeris.

Each record in Fig. 10 has been multiplied by the radial distance x. The Rayleigh wave is dying off proportional to $1/x$. The ratio of radial to vertical displacement is about 0·67 and is very close to the theoretical value for locked Rayleigh waves of 0·68 (for Poisson's ratio of 0·25). The P pulse is decaying faster than $1/x$ because of the behaviour of the directivity function (see Knopoff *et al.* 1957).

For economical computation of such arrivals, it is very important to be able to sample the time function at irregular intervals. The interval should be very short near the P wave and Rayleigh wave arrivals but may be much longer for the rest of the response.

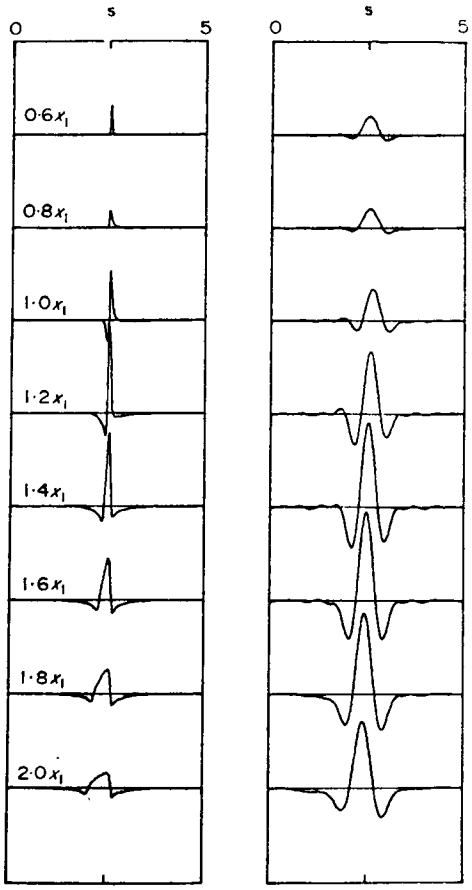

FIG. 8. Potential responses of a layer with a small velocity jump that is inside a shadow zone. The responses correspond to the solid Cagniard paths in Fig. 5.

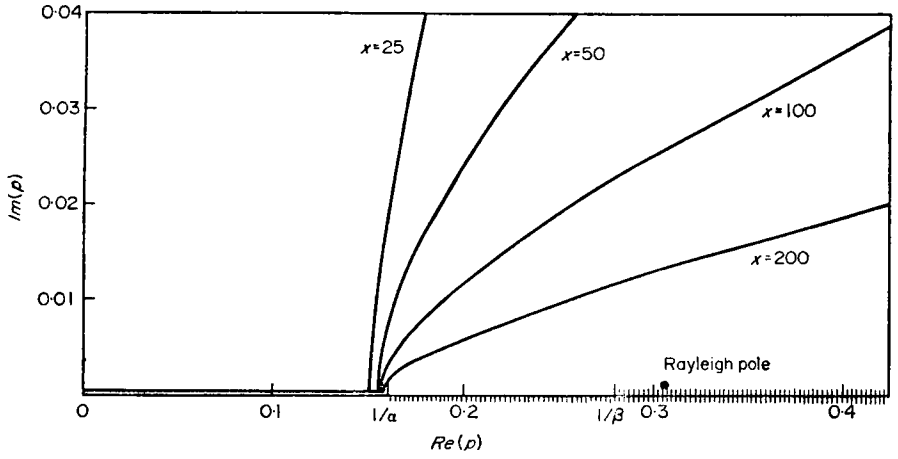

FIG. 9. Cagniard paths, branch cuts and Rayleigh pole for the computation of a *P* first arrival and the Rayleigh arrival for an infinite half space.

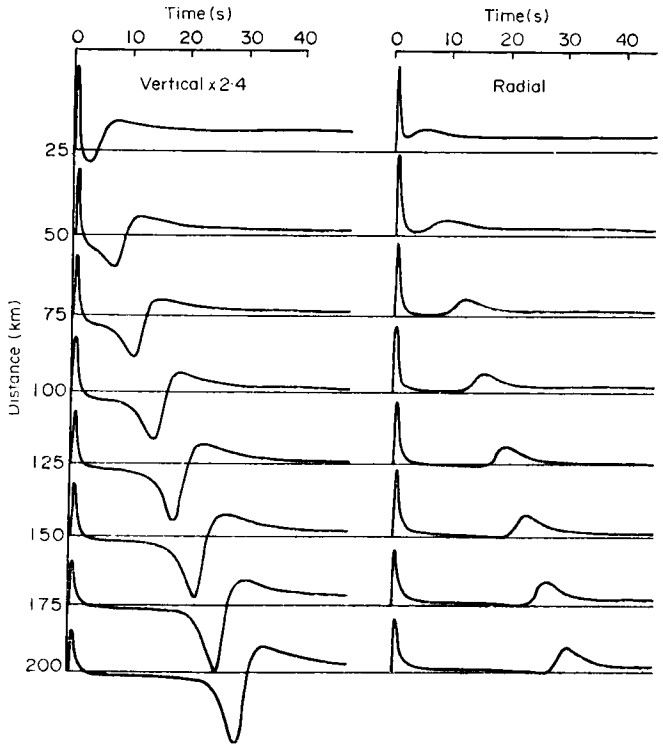

FIG. 10. Vertical and radial displacement responses corresponding to the Cagniard paths shown in Fig. 9.

Approximations

The efficiency of the computation of complete short-period synthetic seismograms for plausible Earth models can be improved considerably by introducing a number of approximations. To illustrate the effects of these approximations we have computed complete responses at several distances for the model shown in Fig. 4.

First let us consider the result of summing the generalized ray responses for all the layers at a particular distance. This process is illustrated in Fig. 11. The principal feature of this seismogram is that the response shape is dominated by the arrivals from the major discontinuities. The arrivals from the many small steps make a significant contribution only if there is constructive interference from nearly simultaneous arrivals.

The seismogram for $\Delta = 18°$ shown in Fig. 11 is repeated in the left two columns of Fig. 12. The seismograms in the two right columns are for $\Delta = 21°$. It is interesting to compare the relative effects of the caustic located between p values of 9·5–10·0 s deg^{-1}. For $\Delta = 18°$ this caustic produces a broad low-frequency arrival spread between 5 and 7 s. For $\Delta = 21°$ the arrivals from the caustic interfere constructively to produce the large first arrival.

The responses (a), (b) and (c) of Fig. 12 show the effect of varying the size of the steps. Although the step-size changes the appearance of the high-frequency plots, the low-frequency displays are all quite similar. One may argue that the 20-km steps are too large even at low frequencies.

The discussion above leads one to suspect that the seismogram shape would not be altered much if non-constructively interfering responses were not included. An easy way of effecting such an exclusion is to include only rays from those layers for

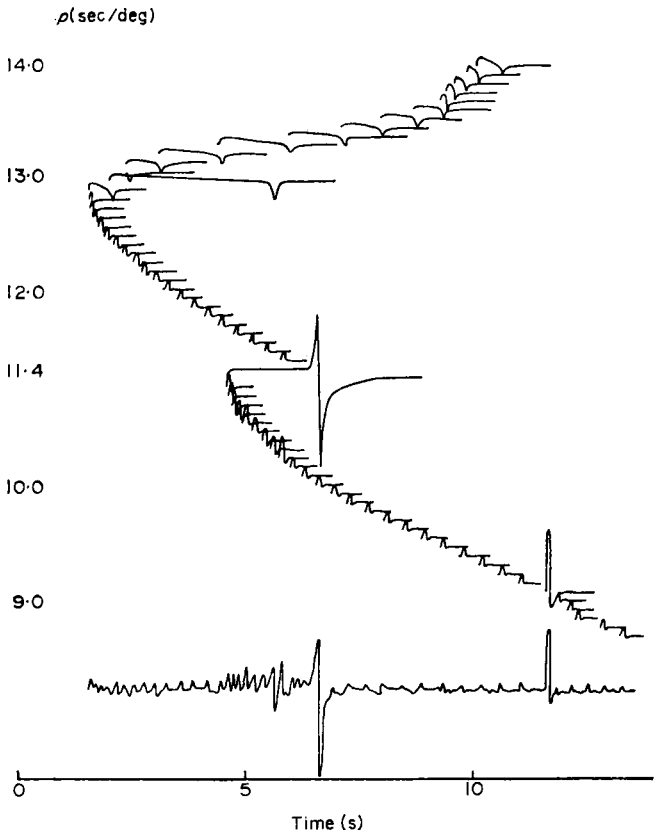

FIG. 11. Illustration of how responses from individual layers are summed to obtain the composite seismogram shown at the bottom. All the responses that were smaller than 10 per cent of the maximum size were enlarged for the individual layer response plots. The model used for these calculations is that shown in Fig. 4.

which the critical distance falls within a certain range from the distance being calculated. Suppose that we are computing a seismogram at distance Δ. If the critical distance for two layers are both located at distance $\Delta - \Delta_c$ then the responses for the rays will interfere constructively. The offset Δ_c is given by the distance between the smooth (p, Δ) curve and the critical distances of the curves corresponding to the model with velocity steps. The example shown in Fig. 4(b) indicates that $\Delta_c \approx 3°$ for 20-km layers. We then exclude any ray that falls outside the window $\Delta - \Delta_c \pm k\Delta_w$ where k is the ratio of the velocity jump of this layer relative to the median velocity jump of the model. The amplitude associated with any particular layer is roughly proportional to the velocity jump at the base of the layer. Thus the inclusion of the factor k means that we take a much wider window for major discontinuities. The responses (d) and (e) in Fig. 12 were computed for $\Delta_w = 5°$ and 2°, respectively. The (d) seismograms are barely distinguishable from those containing all possible rays. The (e) seismograms are almost acceptable except for the first arrival at $\Delta = 18°$. The $\Delta_w = 5°$ window excluded from 40 to 83 per cent of the responses; the $\Delta_w = 2°$ window excluded from 50 to 93 per cent of the responses depending on the distance for which the calculation was made.

The discussion above is concerned entirely with primary reflections. It is important, of course, to also consider the effect of multiple reflections. The (f) responses are the

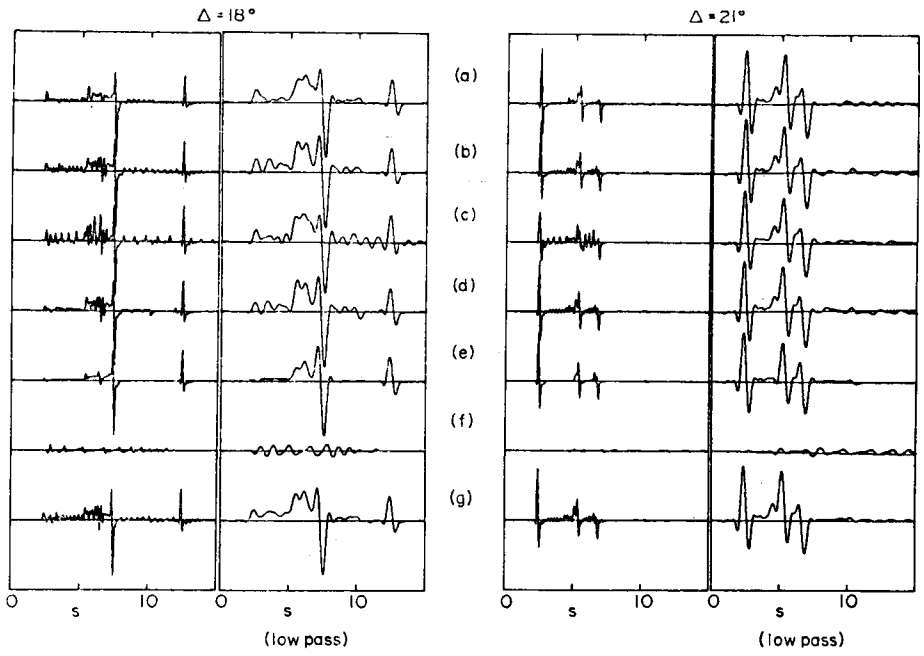

FIG. 12. Illustration of composite seismograms for $\Delta = 18°$ and 21°. The low-frequency versions were obtained by low-pass filtering with a cutoff of 1 Hz. The responses (a), (b) and (c) were obtained by summing the primary reflection from models with 5-, 10- and 20-km steps respectively. The responses (d) and (e) were obtained by deleting certain responses by setting $\Delta_w = 5°$ and 2°, respectively (see text for definition of Δ_w). The responses (f) are first multiples and the responses (g) are primaries and first multiples. The responses (d), (e), (f) and (g) were all computed for models with 10-km steps.

first multiples for a model with 10-km layers. To estimate the contribution of first multiples, we included all rays that are reflected twice at each layer and once at any of the layers above. The (g) responses show the effect of summing the multiples with the primaries. The seismograms with multiples are barely distinguishable from those without. Other experiments indicate that multiples were somewhat larger for 20-km layers and were very much smaller for 5-km layers. Thus we conclude that multiples may be important only for reflections between major discontinuities.

A major cost in the computation of ray responses for models with many layers is involved in the computation of the transmission coefficients $T_j(p)$. Since these coefficients do not vary rapidly with changing p we have found that an excellent approximation is to compute only $T_j(p_0)$ and assume that it remains constant for the entire ray. Computational experiments indicate that the amplitudes determined may be in error by 2–3 per cent with this approximation. The seismogram shapes were indistinguishable from those shown in Fig. 12.

An even cheaper approximation is to assume that for all transmissions $T_j = 1$. This may result in amplitude errors of as much as 10 per cent for short-period responses. The error may be much larger for long-period calculations. An intermediate approach would be to compute the transmission coefficients only at the major discontinuities.

The final approximation does not improve the efficiency of the calculations in any way but is quite revealing about the physics of body-wave propagation. In addition to specifying the P wave velocity model, one must also specify the density

and S wave velocity models. For the examples shown here, we selected a representative density model and an S model that has the same Poisson's ratio as standard Earth models. To check the influence of the density model on the results we replaced the standard model with a model having a uniform density of $\rho = 1\,\mathrm{g\,cm^{-3}}$. The change in maximum amplitude was less than 0·5 per cent and the response shapes were indistinguishable! In the next experiment we kept the uniform density and replaced the S wave velocity model with one having a constant velocity $\beta = 1\,\mathrm{km\,s^{-1}}$. In this case the overall amplitude changed by less than ± 5 per cent, and once again the shapes were indistinguishable. In fact, nearly all of the amplitude variation could be traced to the directivity function $\mathscr{F}_i$. Thus we are led to the conclusion that since the seismogram shape is dominated by arrivals coming from near the critical distance, the reflection coefficients for rays near the critical distance are not dependent on either ρ or β.

Acknowledgments

This research was supported in part by the National Research Council of Canada and in part by the Advanced Research Projects Agency of the Department of Defense of the United States of America and was monitored by the Air Force Office of Scientific Research under contract number F44620-72-C0078.

R. A. Wiggins:
Department of Physics,
University of Toronto,
Toronto M5S 1A7, Canada.

D. V. Helmberger:
Seismological Laboratory,
California Institute of Technology,
Pasadena, California 91109,
U.S.A.

References

Barker, T., 1970. *Response of an elastic layer over an elastic halfspace to a point source*, M.Sc. Thesis, Massachusetts Institute of Technology.

Biswas, N. N. & Knopoff, L., 1970. Exact earth-flattening calculations for Love waves, *Bull. seism. Soc. Am.*, **64,** 1123–1137.

Cagniard, L., 1939. *Reflexion et refraction des ondes seismiques progressives*, Gauthier-Villars, Paris.

Cagniard, L., 1962. *Reflection and refraction of progressive seismic waves*, translated and revised by E. A. Flinn & C. H. Dix, McGraw–Hill, New York.

Červený, V. & Ravindra, R., 1971. *Theory of seismic head waves*, University of Toronto Press, 312 p.

Chapman, C. H., 1973. The earth flattening transformation in body wave theory, *Geophys. J. R. astr. Soc.*, **35,** 55–70.

Cisternas, A., Betancourt, O. & Leiva, A., 1973. Body waves in a 'real earth'. Part I, *Bull. seism. Soc. Am.*, **63,** 145–156.

Fuchs, K. & Müller, G., 1971. Computation of synthetic seismograms with the reflectivity method and comparison with observations, *Geophys. J. R. astr. Soc.*, **23,** 417–433.

Gerver, M. & Markushevich, V., 1966. Determination of a seismic wave velocity from the travel-time curve, *Geophys. J. R. astr. Soc.*, **11,** 165–173.

Gilbert, F. & Helmberger, D. V., 1972. Generalized ray theory for a layered sphere, *Geophys. J. R. astr. Soc.*, **27,** 57–80.

Gilbert, F. & Knopoff, L., 1961. The directivity problem for a buried line source, *Geophysics*, **26,** 626–634.

Helmberger, D. V., 1967. *Head waves from the oceanic Mohorovicic discontinuity*, Ph.D. thesis, UCSD, La Jolla, Calif., 177 pp.

Helmberger, D. V., 1968. The crust-mantle transition in the Bering Sea, *Bull. seism. Soc. Am.*, **58**, 179–214.

Helmberger, D. V., 1972. Long-period body-wave propagation from 4° to 13°, *Bull. seism. Soc. Am.*, **62**, 325–341.

Helmberger, D. V. & Wiggins, R. A., 1971. Upper mantle structure of midwestern United States, *J. geophys. Res.*, **76**, 3229–3245.

Hoop, A. T., de, 1960. A modification of Cagniard's method for solving seismic pulse problems, *Appl. Sci. Res.*, **B8**, 349–356.

Knopoff, L., Fredricks, R. W., Gangi, A. F. & Porter, L. D., 1957. Surface amplitudes of reflected body waves, *Geophysics*, **22**, 842–847.

Lamb, H., 1904. On the propagation of tremors over the surface of an elastic solid, *Phil. Trans. R. Soc. Lond.*, **A203**, 1–42.

Müller, G., 1970. Exact ray theory and its application to the reflection of elastic waves from vertically inhomogeneous media. *Geophys. J. R. astr. Soc.*, **21**, 261–283.

Müller, G., 1971. Approximate treatment of elastic body waves in media with spherical symmetry, *Geophys. J. R. astr. Soc.*, **23**, 435–450.

Müller, G., 1973. Theoretical body wave seismograms for media with spherical symmetry; discussion and comparison of approximate methods, *Z. Geophys.*, **39**, 229–246.

Pekeris, C. L., Alterman, Z., Abramovici, F. & Jaroisch, H., 1965. Propagation of a compressional pulse in a layered solid, *Rev. Geophys.*, **3**, 25–47.

Shanks, J. L., 1967. Recursive filters for digital processing, *Geophysics*, **32**, 789–800.

Sommerfeld, A., 1909. Uber die Ausbreitung der Wellen in der drahtlosen Telegraphie, *Ann. Physik*, **28**, 665–736.

Stockham, T. G., 1969. High speed convolution and correlation with applications to digital filtering, in Gold, B. & Rader, C. M., *Digital processing of signals*, pp. 203–232, McGraw–Hill, New York.

Strick, E., 1959. Propagation of elastic wave motion from an impulsive source along a fluid/solid interface, II: Theoretical pressure pulse, *Phil. Trans. R. Soc. Lond.*, **A251**, 465–523.

Wiggins, R. A. & Helmberger, D. V., 1973. Upper mantle structure of western United States, *J. geophys. Res.*, **78**, 1870–1880.